Human Molecular Genetics, 2009, Vol. 18, No. 7 ***1252–1265***
doi:10.1093/hmg/ddp025
Advance Access published on January 15, 2009

Loss of *Tsc2* in radial glia models the brain pathology of tuberous sclerosis complex in the mouse

Sharon W. Way, James McKenna III, Ulrike Mietzsch, R. Michelle Reith, Henry Cheng-ju Wu and Michael J. Gambello*

Division of Medical Genetics, Department of Pediatrics, University of Texas Health Science Center, 6431 Fannin Street, MSB 3.144, Houston, TX 77030, USA

Received December 15, 2008; Revised December 15, 2008; Accepted January 12, 2009

Tuberous sclerosis complex (TSC) is an autosomal dominant, tumor predisposition disorder characterized by significant neurodevelopmental brain lesions, such as tubers and subependymal nodules. The neuropathology of TSC is often associated with seizures and intellectual disability. To learn about the developmental perturbations that lead to these brain lesions, we created a mouse model that selectively deletes the *Tsc2* gene from radial glial progenitor cells in the developing cerebral cortex and hippocampus. These *Tsc2* mutant mice were severely runted, developed post-natal megalencephaly and died between 3 and 4 weeks of age. Analysis of brain pathology demonstrated cortical and hippocampal lamination defects, hippocampal heterotopias, enlarged dysplastic neurons and glia, abnormal myelination and an astrocytosis. These histologic abnormalities were accompanied by activation of the mTORC1 pathway as assessed by increased phosphorylated S6 in brain lysates and tissue sections. Developmental analysis demonstrated that loss of Tsc2 increased the subventricular Tbr2-positive basal cell progenitor pool at the expense of early born Tbr1-positive post-mitotic neurons. These results establish the novel concept that loss of function of *Tsc2* in radial glial progenitors is one initiating event in the development of TSC brain lesions as well as underscore the importance of Tsc2 in the regulation of neural progenitor pools. Given the similarities between the mouse and the human TSC lesions, this model will be useful in further understanding TSC brain pathophysiology, testing potential therapies and identifying other genetic pathways that are altered in TSC.

INTRODUCTION

The autosomal dominant tumor suppressor disorder, tuberous sclerosis complex (TSC), bears its name from the tuber-like brain lesions described by Desire-Magloire Bourneville in the late 1800s (1). Most affected patients have a germline inactivating mutation of either *TSC1* or *TSC2*, encoding the proteins hamartin and tuberin, respectively (2,3). Loss of the second allele, leading to loss of heterozygosity (LOH), has been shown to predispose to tumor formation in many organs (4,5). Although any organ can be affected, the brain, skin, kidney, lung and heart are principal sites of pathology (6). The effects of TSC on the brain are particularly debilitating, encompassing a variety of lesions such as cortical tubers, subependymal nodules, white matter linear migration lines, corpus callosum abnormalities and transmantal cortical dysplasia associated with hemimegalencephaly (7). The histopathology of tubers is characterized by generalized cellular disorganization, astrocytosis and characteristic giant cells. The neuropathology of TSC is associated with epilepsy, developmental delay, behavioral abnormalities and autism spectrum disorders (8–10). Because the neurologic sequelae of TSC cause significant morbidity and mortality, there is intense interest in understanding and treating the brain manifestations of this disease.

Hamartin and tuberin form a biochemical TSC complex that inhibits the insulin- and nutrient-induced mTOR/S6K/4E-BP1 signal transduction pathway that controls translation,

*To whom correspondence should be addressed. Tel: +1 713 500 5760; Fax: +1 713 500 5689; Email: michael.j.gambello@uth.tmc.edu

proliferation and cell growth (11–13). This inhibition is mediated primarily through the GTPase activity of the TSC complex toward Rheb-GTP, a small Ras-like protein (14,15). Rheb-GTP normally activates the rapamycin-sensitive mTOR complex, called mTORC1, in which the mTOR kinase is associated with the proteins raptor and GβL (16,17). Loss of either TSC1 or TSC2 in TSC abolishes Rheb-GTPase activity, resulting in constitutively activated mTORC1. Activated mTORC1 kinase leads to increased levels of several phosphorylated proteins of the translational apparatus, such as S6 kinase and ribosomal protein S6. The end result is increased translation, cell size and proliferation. The giant cells of tubers stain intensely for both phosphorylated S6 kinase and phosphorylated S6, indicating that mTORC1 activation is an important mechanism for TSC neuropathology (5,18). The identification of the TSC1–TSC2 complex as an inhibitor of mTORC1 has paved the way for a novel medical treatment of TSC. The fungal metabolite rapamycin, which is widely used to suppress the immune system in organ transplant patients, inhibits mTORC1 activity (19). The mTORC1-inhibitory function of rapamycin led to the hypothesis that rapamycin might be able to restore the inhibition lost in TSC. Subsequent cell culture and animal studies confirmed that hypothesis (20–23). It has recently been demonstrated that rapamycin can rescue the seizure phenotype in an astrocyte-specific *Tsc1* mouse model (24). Rapamycin also improved survival and rescued cell size and myelination abnormalities in a neuronal-specific *Tsc1* model of TSC (25). Indeed, rapamycin appears to be very promising for the treatment of TSC, and several human trials have already yielded encouraging results (26,27). In spite of the recent discoveries regarding the functions of hamartin and tuberin, the pathophysiology of TSC brain lesions remains poorly understood. Most brain lesions are present at birth, suggesting that the neuropathology of TSC represents developmental defects (1,7). Tubers have been detected *in utero* using high-resolution ultrasound and fetal MRI (18,28). Neuroglial progenitor markers, vimentin and nestin, have been demonstrated in the cells of tubers (29,30). These observations have led to a prevailing hypothesis that neuroglial precursor cells might be the cells of origin of the brain lesions of TSC (18,31). This hypothesis remains untested.

Initial attempts to model TSC in the mouse did not result in significant TSC-like brain pathology. Mice with heterozygous disruptions of *Tsc1* or *Tsc2* developed kidney and liver lesions, but limited brain pathology (22,32–35). Homozygous deletion of either gene caused midgestation lethality, possibly related to liver hypoplasia, though some embryos had exencephaly. Recent models using a conditional allele of the *Tsc1* have been more fruitful. Conditional disruption of *Tsc1* in astrocytes, using a GFAP-Cre driver, produced mice that demonstrated enlarged brains, an astrocytosis and mTORC1 activation (36). $Tsc1^{flox/flox}$;*GFAP-Cre* mice had normal cortical organization, mild hippocampal abnormalities and died from seizures by 3 months of life. Generation of a neuron-specific deletion of *Tsc1* using a synapsin-Cre driver also produced severely compromised animals that died within a few months of life from seizures (37,38). There is some discrepancy as to whether these animals exhibit histologic abnormalities in the cerebral cortex or hippocampus; however, they clearly demonstrate enlarged neurons, activated mTORC1 and myelination defects. Although these *Tsc1*-based models do not demonstrate tubers or subependymal nodules *per se*, they exhibit significant features of the human disease and will be useful to dissect out the functions of the TSC complex in different neuronal populations. Nonetheless, neither model has tested the hypothesis that loss of *Tsc1* or *Tsc2* in a neuroprogenitor cell initiates TSC neuropathology. Moreover, these studies are all based upon the *Tsc1* gene. Although patients with TSC can have mutations in either gene, *TSC2*-based disease appears to be more severe and causes more profound central nervous system (CNS) dysfunction (39,40). Therefore, in an effort to develop a *Tsc2*-based model for TSC neuropathology, we have created a conditional allele of *Tsc2* in the mouse (41). Our goal was to use this floxed allele to delete *Tsc2* in a neuroglial progenitor population to recapitulate the brain manifestations of TSC.

Over the past several years, the traditional function of radial glial cells as a mere scaffold for migrating and developing neurons has been expanded to that of neuroglial precursor cells (42). Multiple lineage tracing experiments using Cre transgenic mice and real-time imaging have demonstrated that radial glial cells likely give rise to a majority of cells in the cerebral cortex (43,44). At midneurogenesis, radial glia can divide symmetrically to generate other radial glia, or asymmetrically to self-renew and produce post-mitotic neurons (45). Some radial glia can also generate a second progenitor pool in the subventricular zone containing neurogenic basal progenitor cells (46,47). At later stages of development, radial glia are primarily gliogenic. Given these neuroglial progenitor properties, we speculated that loss of *Tsc2* in radial glial might recapitulate the brain pathology of TSC. We used an extensively characterized *hGFAP-Cre* mouse (48–50) to remove the *Tsc2* gene from radial glial progenitor cells. The *hGFAP-Cre* transgenic is notably very different from the GFAP-Cre used to create the astrocyte-specific *Tsc1* knockout model (36). In the *hGFAP-Cre* mouse, Cre recombinase is expressed in the radial glia of the hippocampal anlage at E12 and in the cortical radial glia at E13.5–14 (48–50). Using the *hGFAP-Cre* mouse allowed us to remove Tsc2 from these progenitor cells and their neuronal and glial progeny, creating a model more similar to the human disease. In the $Tsc1^{flox/flox}$;*GFAP-Cre* mouse, Cre was only expressed in astrocytes, consequently leaving normal Tsc1 function in all neurons. We generated $Tsc2^{flox/ko}$;*hGFAP-Cre* mice to mimic TSC patients with heterozygous loss of *TSC2* in all cells and selective loss of the remaining copy of *Tsc2* only in radial glial cells. This strategy allowed us to bypass the lethality of homozygous knockouts and create a novel *Tsc2*-based model of TSC that recapitulates many features of the human disease in the brain. Our data demonstrate new roles of the TSC complex in radial glial biology and cerebral cortical development.

RESULTS

Generation of $Tsc2^{flox/ko}$;*hGFAP-Cre* mice

We crossed male $Tsc2^{+/ko}$;*hGFAP-Cre* mice with female $Tsc2^{flox/flox}$ mice to generate the desired progeny, $Tsc2^{flox/ko}$;

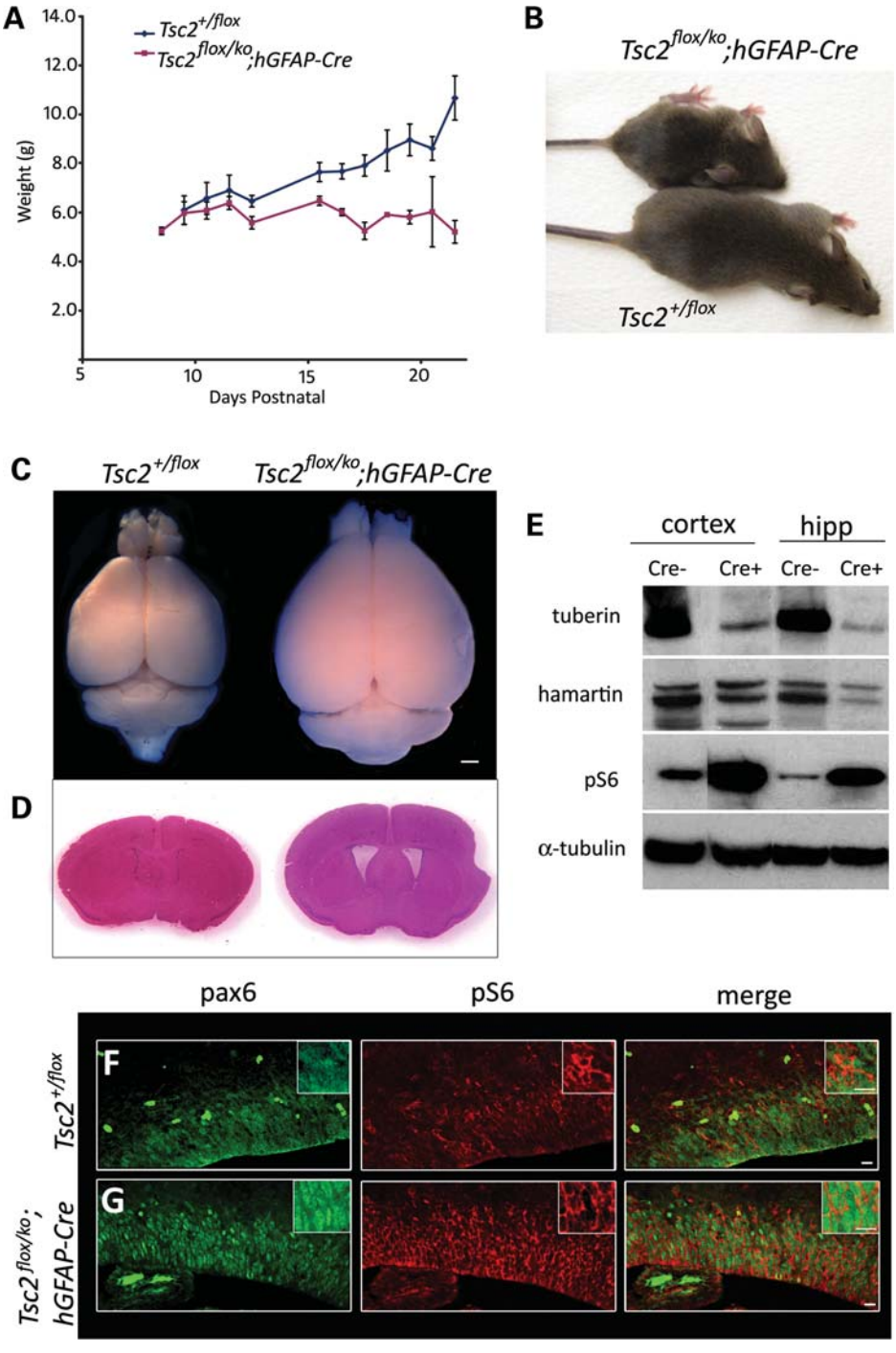

Figure 1. Generation of *Tsc2*$^{flox/ko}$*;hGFAP-Cre* mice. **(A)** Weight curves of mutant (*Tsc2*$^{flox/ko}$*;hGFAP-Cre*) mice (red, $n = 17$) compared with the control (*Tsc2*$^{+/flox}$) mice (blue, $n = 15$) demonstrating the retarded growth of the mutant animals. **(B)** A runted mutant, 21-day-old (P21) mouse compared with a control littermate. Note the domed head and splayed feet in the mutant animal. **(C)** The brain of the mutant mouse (right) was noticeably larger than the control (left). **(D)** Ventricles in the mutant mouse were dilated (right). **(E)** Immunoblot analyses of cortical and hippocampal lysates from mutant ('Cre+') mice demonstrated a marked decrease of tuberin, slightly decreased levels of hamartin and large increase in pS6 levels compared with the control ('Cre-'). α-Tubulin was used as the loading control. **(F** and **G)** Pax6 and pS6 immunohistochemistry in E15.5 control (F) and mutant (G) mice showed increased activation of mTORC1 in the radial glial cells of the developing cortex. Scale bars, C, 1 mm; F and G, 10 μm.

hGFAP-Cre. These mutant mice represented TSC patients with one inactivated *Tsc2* allele in all cells. Cre expression only occurred in radial glial cells; hence, the second floxed allele was only lost in radial glial cells and their neuronal and glial descendents. This scheme also tested whether the two hit hypothesis is operative in TSC neuropathology, a somewhat controversial issue (51,52). *Tsc2*$^{flox/ko}$*;hGFAP-Cre* mice were born in the expected Mendelian ratio and appeared healthy until

about post-natal day 8, when their weight gain slowed compared with littermate controls (Fig. 1A). By weaning, *Tsc2*$^{flox/ko}$*;hGFAP-Cre* mice were severely runted (Fig. 1B) and died between 3 and 4 weeks, likely from seizures, as we observed several mice seizing ($n = 6$) and the majority of dead mice were found in extensor posturing. The *Tsc2*$^{flox/ko}$*;hGFAP-Cre* mice had splayed feet, domed heads, and were often tremulous and generally less active than littermate controls. Because mutant animals were often quite sick at weaning and died during the week after, all analyses on adult mice were conducted at post-natal day 21 (P21). The brains of the *Tsc2*$^{flox/ko}$*;hGFAP-Cre* mice were substantially larger than control brains and demonstrated dilated lateral ventricles (Fig. 1C and D). In the *Tsc2*$^{flox/ko}$*;hGFAP-Cre* mice, Cre recombinase deleted the floxed *Tsc2* allele in the majority of radial glia in the hippocampal anlage at E12.5 and in the cortical ventricular zone at E13.5–14 (49,50). Consequently, all the neurons and astrocytes derived from *Tsc2*-null radial glia should have had complete loss of tuberin antigen. To demonstrate extensive loss of tuberin, western analysis of cell lysates from P21 cortex and hippocampus of the *Tsc2*$^{flox/ko}$*; hGFAP-Cre* and control mice was performed and demonstrated significant loss of tuberin antigen (Fig. 1E). Hamartin levels were also slightly decreased in experimental lysates, reflecting the dependence of its stability on the presence of its binding partner tuberin (53). Loss of tuberin antigen was accompanied by an expected activation of the mTORC1 pathway based on increased levels of phosphorylated (Ser 240/244) S6 (pS6). We then demonstrated that mTORC1 was activated in radial glia by performing immunohistochemistry on E15.5 brains using antibodies against the radial glial marker Pax6 and pS6 (Fig. 1F and G) (54). In the mutant embryonic brains, more intensely red pS6 staining was seen surrounding the green Pax6-labeled nuclei of radial glial cells in the ventricular zone compared with the control. This increased pS6 expression in radial glial cells demonstrated activation of mTORC1 caused by loss of *Tsc2*.

Loss of Tsc2 in radial glia causes cortical and hippocampal enlargement, enlarged cells, lamination defects, heterotopias and activated mTORC1 in neurons and glia

Histologic analysis of P21 mice revealed a thicker cerebral cortex from rostral to caudal telencephalon, a blurring of the gray–white junction, a smaller marginal zone (Layer I) and apparent lamination defects (Fig. 2A and B) in the mutant. Higher magnification demonstrated many cells with enlarged somata and nuclei, and more extracellular matrix in the mutant compared with the control (Fig. 2C and D). The loss of Tsc2 in radial glia should have activated mTORC1 in all their neuronal and glial progeny, similar to what has been observed in human TSC lesions (18,55). To assess cortical neuronal and astrocyte mTORC1 activation, we performed double immunohistochemistry against NeuN, a neuronal marker, or S100, an astrocyte marker, and pS6. In the rostral cerebral cortex, almost all NeuN-positive cells in the mutant demonstrated increased pS6 antigen (Fig. 2F and G). Note the increased size ($P < 0.005$) of almost all the mutant neurons compared with the control (Fig. 2E). Similarly, the S100-positive astrocytes in the rostral cortex of mutant mice were larger and expressed more pS6 than those of control animals (Fig. 2H and I).

The hippocampus of mutant *Tsc2*$^{flox/ko}$*;hGFAP-Cre* mice also demonstrated defects in organization. There were lamination defects throughout the pyramidal layer, most severe in regions CA1 and CA3 (Fig. 3B), with many ectopic, enlarged neurons in the stratum oriens (SO) (Fig. 3F and G). These defects were in stark contrast to the tight, ordered pyramidal layer of the control animals, with a relatively cell sparse SO (Fig. 3A and E). The dentate gyrus (DG) retained its overall structure and contained approximately equal numbers of granule cells. However, in the mutant hippocampus, there were large, ectopic granule cells lining the outer limit of this region (Fig. 3C and D). Another striking defect was the presence of ring heterotopias throughout the stratum lacunosum moleculare (SLM) (Fig. 3B and H). These heterotopias were mainly composed of NeuN-positive neurons with a few enlarged S100-positive astrocytes (Fig. 3I and J). There were, however, several DAPI-stained nuclei that were neither NeuN nor S100 positive, suggesting that differentiation into a neuronal or glial lineage was abnormal. Hippocampal NeuN-positive cells and S100-positive cells also demonstrated increased pS6 (Fig. 3K, L, N and O). However, the DG of both mutant and control hippocampus did not express a similar increase in the intensity of pS6 antigen compared with respective pyramidal layers (PL). Previous studies have verified that Cre is expressed in DG granule cell precursors in the *hGFAP*-Cre transgeneic mouse (49,50). Therefore, we postulated that increased mTORC1 activity in granule cells of the DG might not result in elevated pS6 levels comparable with the pyramidal cell layer. Nonetheless, mTORC1 activation should result in an increase in cell size, so we compared the areas of DG granule cells between mutant and control animals (Fig. 3M). Granule cells from the mutant DG were on average 10% larger ($P < 0.0005$) than those in the control DG, suggesting that *Tsc2* deletion and mTORC1 activation occurred in the DG of the mutant. Together, these results indicated that mTORC1 remained activated in the neurons and astrocytes derived from Tsc2-deficient radial glia. This mTORC1 activation resulted in increased cell size, both in the cortex and in the hippocampus, as previously reported in several model systems (31,37).

Developmental analysis of *Tsc2*$^{flox/ko}$*;hGFAP-Cre* mice reveals post-natal cerebral enlargement and possible migration defects

To analyze the development of the cerebral abnormalities seen at P21, we examined hematoxylin and eosin (H&E) stained sections from E16.5–P15 (Fig. 4). At E16.5, we observed no notable difference in thickness of the developing cortex between mutant and control (data not shown). At P0, the difference in thickness of the cerebral cortex was also minimal, though the ventricular zone appeared thicker in the mutant (Fig. 4A and B). In the hippocampus, defects in organization of the CA3 layer of the mutant were already apparent (Fig. 4C and D). By P5, the difference in cortical thickness became more pronounced while the lamination abnormalities in CA1 and CA3 and ectopic neurons in the SO were

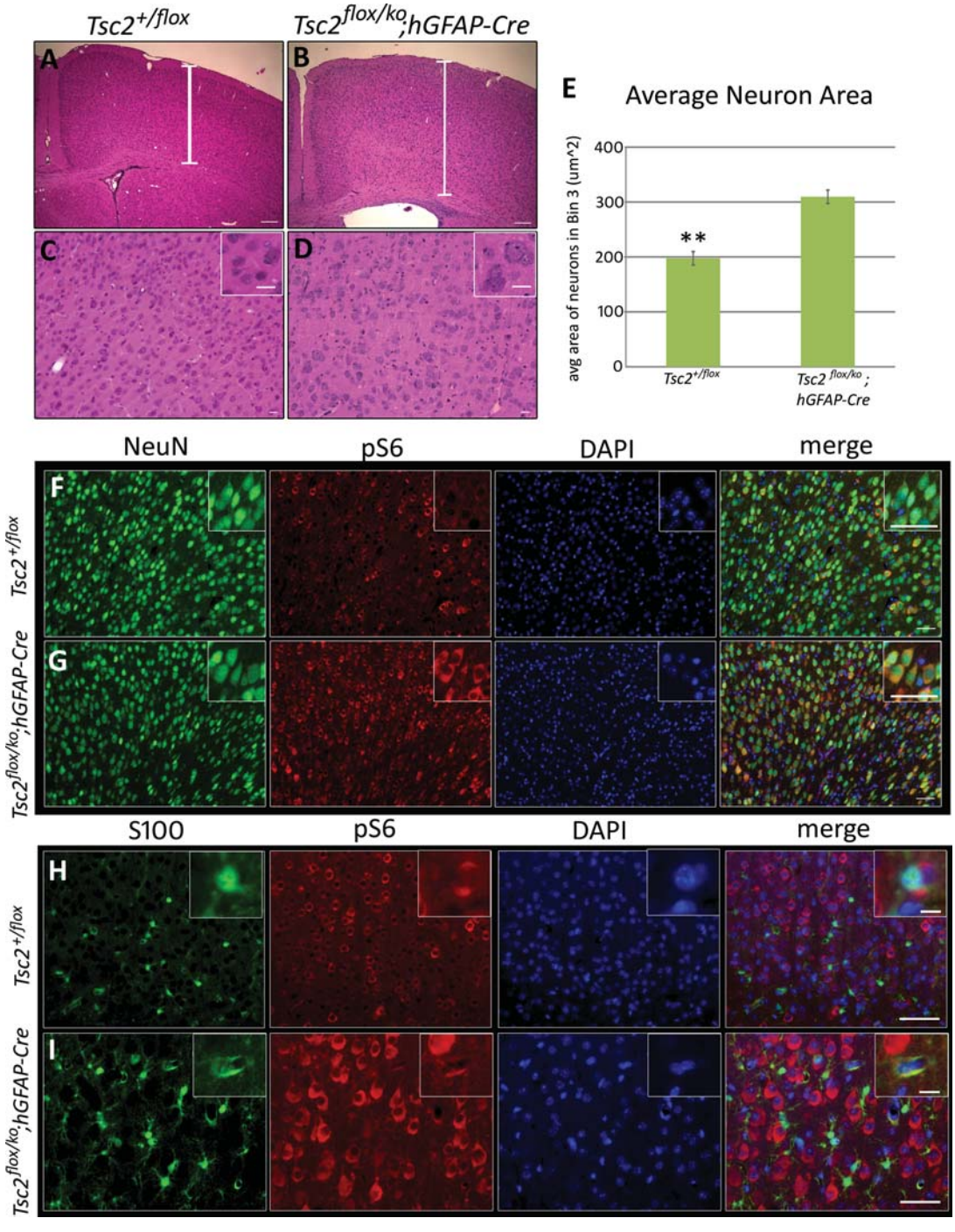

Figure 2. Cerebral cortical defects and up-regulation of mTORC1 in cortical neurons and astrocytes in *Tsc2$^{flox/ko}$;hGFAP-Cre* mice. All sections were taken from P21 mice. **(A** and **B)** The cortex of the mutant (B) was thicker than the control (A) and displayed lamination defects, blurring between the gray–white junction, and a much less-defined molecular layer (Layer I). **(C** and **D)** Higher magnification revealed enlarged cells in the cortex of the mutant (D) and more extracellular matrix between the cells compared with the control (C). **(E)** Comparison of the areas of NeuN-labeled neurons from mutant and control cortex revealed that mutant neurons are significantly larger ($^{**}P < 0.005$, $n = 6$) than control neurons. **(F** and **G)** NeuN-labeled neurons in the mutant cortex (G) displayed substantial increase in pS6 expression compared with the control (F), indicating elevated mTORC1 activation. **(H** and **I)** S100-labeled astrocytes in the mutant cortex (I) also showed notable increase in pS6 expression compared with the control (H). Scale bars, A and B, 100 μm; C and D, 20 μm; F and G, 50 μm; H and I, 40 μm, inset 10 μm.

evident. In the hippocampal fissure, there were several ectopic clusters of cells in the mutant brains (Fig. 4E–H). These clusters appeared to be the site of origin of the future ring heterotopias. By P10, the mutant cortex was noticeably thicker than control and the ring heterotopias were becoming more obvious (Fig. 4I–M). By P15, the mutant brains were similar histologically to brains analyzed at P21 (Fig. 4N–Q).

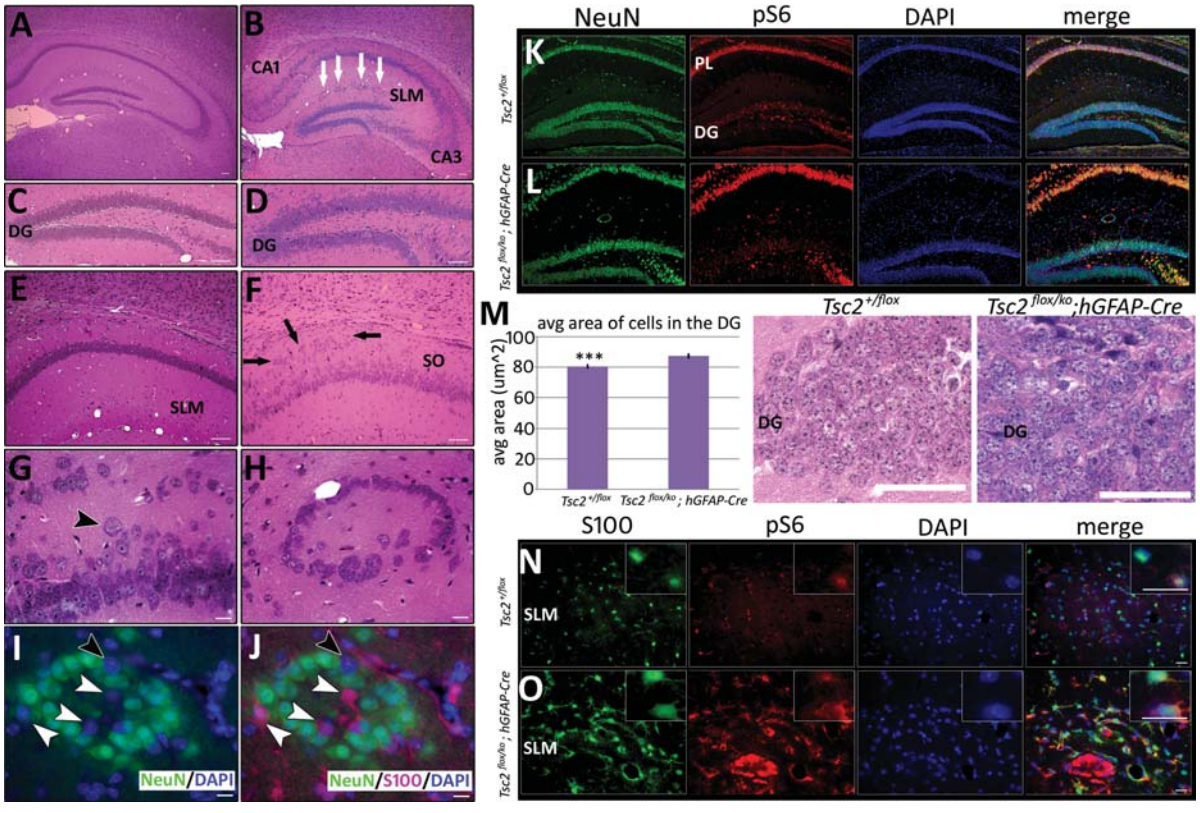

Figure 3. Hippocampal defects and up-regulation of mTORC1 in hippocampal neurons and astrocytes in *Tsc2$^{flox/ko}$;hGFAP-Cre* mice. All sections were taken from P21 mice. **(A** and **B)** Severe lamination defects in the mutant mouse (B) were apparent in H&E-stained sections of the hippocampus, especially in the CA1 and CA3 regions. White arrows represent ring heterotopias that were evident throughout the SLM. **(C** and **D)** The DG was lined with large, ectopic granule cells in the mutant (D). **(E**–**G)** Numerous ectopic neurons (F, black arrows) and enlarged cells (G, black arrowhead) were also present in the SO of the mutant hippocampus (F), in contrast to the tight, well-organized pyramidal layer in the control (E). **(H**–**J)** High power magnification of a ring heterotopia demonstrated that they were mainly composed of NeuN-positive neurons (green cells) with some S100-positive astrocytes (I, J, red cells, white arrowheads), though some cells do not stain for either marker (I, J, black arrowheads). **(K** and **L)** NeuN-labeled neurons in the hippocampus of the mutant (L) displayed greater pS6 expression than the control (K). However, expression of pS6 in the DG of both the mutant and the control is reduced compared with their respective PL. **(M)** Despite low immunohistochemical pS6 expression in the mutant DG, average cell area of cells in the DG of the mutant was significantly larger ($^{***}P < 0.0005$) than the control ($n = 6$). **(N** and **O)** S100-labeled astrocytes in the hippocampus of the mutant (O) had increased pS6 expression. The SLM region of the hippocampus is shown. Scale bars, A–F, 50 μm; G–J, 10 μm; K and L, 100 μm; M, 50 μm; N and O, 20 μm.

Loss of Tsc2 in radial glia causes perturbations in neuronal subsets and an astrogliosis

To gain further insight into the enlarged brains of the mutant animals, we assessed cortical lamination with layer-specific immunohistochemistry. Antibody to Cux-1 labels neurons in Layers II–IV of the mammalian cerebral cortex (Fig. 5A) (56). In the *Tsc2$^{flox/ko}$;hGFAP-Cre* cortex, labeled Cux1 cells were not restricted to Layers II–IV, but detected throughout the entire cortex. Moreover, though the difference was not found to be significant (Fig. 5D), there was a slight increase in Cux-1 positive neurons in the mutant cerebral cortex compared with the control. The integrity of Layer VI was assessed using antibody against the transcription factor FoxP2 (Fig. 5B) (57). In the mutant cortex, there was a well-demarcated FoxP2-positive Layer VI; however, there were ∼30% less FoxP2-positive cells ($P < 0.05$) in the mutant Layer VI than the control. TUNEL analysis at E16.6 and P10 suggested that the fewer FoxP2 cells were not due to increased cell death (data not shown). Since there were significantly fewer FoxP2-labeled neurons, and because the macrocephaly occurred post-natally, we asked whether the total number of NeuN-positive neurons or S100-positive glia in the cerebral cortex of the mutant animals were different. Quantitation of both cell populations did not reveal a significant difference between the total number of NeuN-positive neurons (Fig. 5C) or of S100-positive glia (Fig. 5H) in the cortex of the control versus mutant animals. Further analysis with PCNA, a proliferation marker, showed no significant difference in PCNA-positive cells in the cortex at P10 (data not shown), in accordance with the total cell counts.

An astrogliosis is often present in TSC tubers (55). Astrogliosis usually occurs when insult to the brain is sustained, yet tubers display alterations in astrocytes, even though no physical damage has occurred. In the synapsin-Cre-based *Tsc1* mouse model, no evidence of astrogliosis was observed (37). GFAP-Cre-driven *Tsc1* deletion in astrocytes did yield an astrogliosis throughout the cortex and the hippocampus (36). To determine whether our conditional deletion of *Tsc2* in radial glia resulted in astrogliosis, we performed immunohistochemistry for GFAP on P21 brains. The normal mouse cerebral cortex expresses very weak GFAP

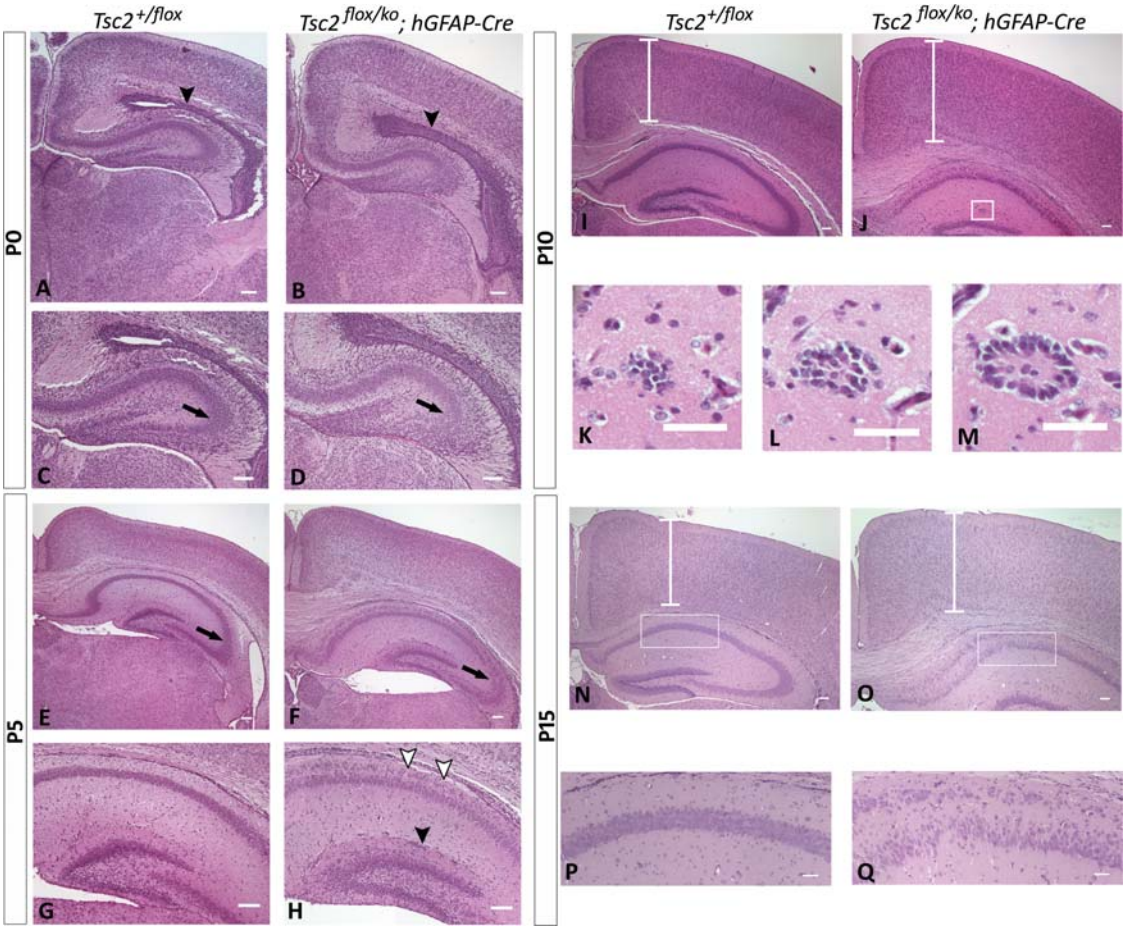

Figure 4. Post-natal developmental analysis of *Tsc2$^{flox/ko}$;hGFAP-Cre* mice. H&E-stained sections from P0 to P15. **(A–D)** At P0, the size of the cerebral cortex was comparable between the control and the mutant. The ventricular zone (arrowheads) appeared thicker in the mutant and lamination abnormalities in CA1 and CA3 (arrows) were beginning to develop. **(E–H)** At P5, an increase in the cortical thickness of the mutant **(F)** was more apparent. The layering abnormalities in CA3 (arrow) were more pronounced. There were many ectopic cells in the SO of the mutant (H, white arrowheads) compared with the control. There was also the appearance of clusters of cells in the hippocampal fissure (black arrowhead). **(I–M)** By P10, the cerebral cortex of the mutant had continued to enlarge, and the layering was indistinct compared with the control. The ring heterotopias in the SLM were evident (inset J). The corpus callosum was also noticeably thicker. Sectioning through a heterotopia (K–M) demonstrated that they represent a nodule of ectopic cells. **(N–Q)** By P15, the same abnormalities were present as those seen at weaning. Scale bars, A, B, E–J, N, O, 100 μm; C, D, K–M, P, Q, 50 μm.

immunostaining, whereas the *Tsc2$^{flox/ko}$;hGFAP-Cre* mutant cortex revealed a marked increase in GFAP expression throughout the entire cortical thickness (Fig. 5F). There was also increased GFAP staining around the mutant ventricular zone surrounding the lateral ventricles. Increased GFAP expression was also seen throughout the hippocampus, where astrocytes in all hippocampal regions, especially the SLM, displayed more intense GFAP expression. The cell bodies of the astrocytes in the mutant were also larger, with shorter and thicker processes than those of the control cells, a characteristic of activated astrocytes (Fig. 5G, inset). Quantitation of GFAP-labeled cells within the hippocampus showed significantly more astrocytes in the mutant (Fig. 5I). The increased number of GFAP-positive cells in the hippocampus was also accompanied by an increase in PCNA-positive cells (data not shown). These results verified that *Tsc2* deletion in radial glia caused an astrogliosis in the cortex mainly by astrocyte activation, but in the hippocampus by both activation and proliferation.

Loss of Tsc2 in radial glia alters progenitor cell populations with minimal effect on proliferation

The equal numbers of NeuN-positive neurons and S100-positive glia between the mutant and the control cerebral cortex suggested that loss of Tsc2 had a minimal effect on proliferation of radial glial cells. To address this, we pulse-labeled E14.5 embryos with BrdU for 30 min before sacrifice to label cells in S phase. Quantitation of BrdU-positive cells revealed no significant difference between control and mutant animals (Fig. 6A–C), suggesting that loss of Tsc2 had a small if any effect on proliferation at this time point. Since we did observe notably fewer FoxP2-labeled early born neurons in the mutant cortex, we reasoned that loss of Tsc2 in radial glia might affect their differentiation into post-mitotic neurons versus subventricular basal progenitor cells. Immunohistochemistry for Tbr2, a marker of basal progenitor cells, demonstrated a significant increase in this progenitor population compared with wild-type ($P < 0.0005$, Fig. 6D–F)

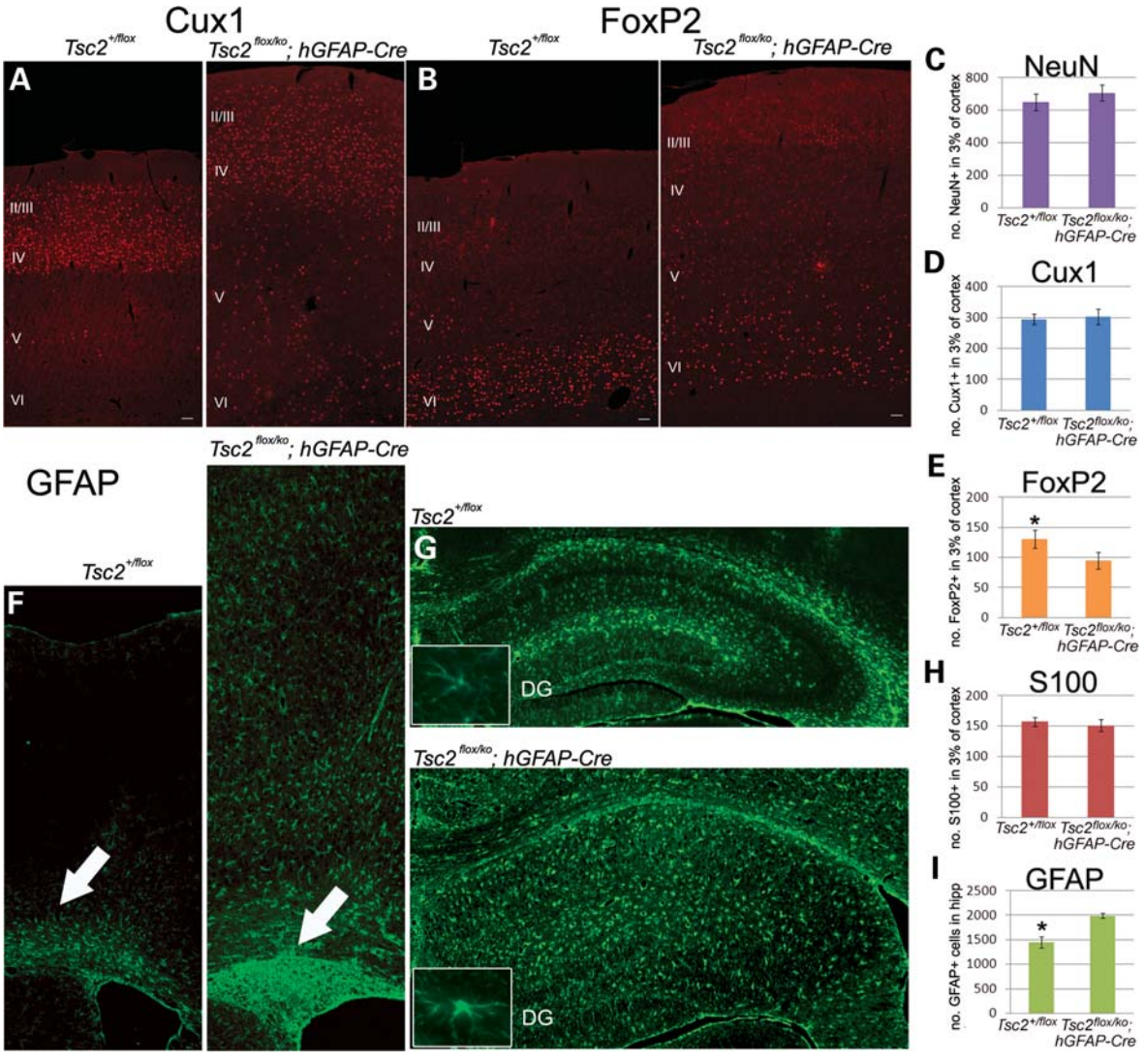

Figure 5. Lamination defects and astrogliosis in the *Tsc2*$^{flox/ko}$*;hGFAP-Cre* mice. All sections and counts conducted in P21 mice. **(A** and **b)** Cux1 (A), a Layer II–IV marker, and FoxP2 (B), a Layer VI marker, were used to assess lamination defects ($n = 6$ and 4, respectively). The Cux1-labeled cells of the control resided mostly in their designated layers, whereas the labeled cells of the mutant were scattered throughout the cortex. FoxP2-labeled cells were generally in Layer VI for both control and mutant. **(C–E)** Although NeuN-labeled neurons (C) and Cux1-labeled cells (D) were not found to be significantly different in the cortex, there were significantly less FoxP2-labeled cells in the mutant (E, $^{*}P < 0.05$). **(F** and **H)** Immunostaining of GFAP in the cortex (F) revealed substantial increase of GFAP-expressing astrocytes in the cortex compared with the control. Intense GFAP expression was also seen in the mutant ventricular zone of the lateral ventricle (white arrows). As quantification of GFAP+ cells in the cortex was difficult in the control, S100 (H) was used to label cortical astrocytes. No significant difference was found in S100+ cells between the mutant and the control. **(G** and **I)** GFAP expression was notably higher in the mutant hippocampus where astrocytes had larger cell bodies but shorter, thicker processes compared with the control. Significantly more GFAP-labeled cells (I) were present in the mutant hippocampus.

(reference Tbr2). We reasoned that an increase in Tbr2-positive basal progenitor cells might be accompanied by a decrease in the number of Tbr1-positive post-mitotic neurons at E14.5 that might explain the lower number of FoxP2-labeled Layer VI neurons. Indeed, Tbr1-positive cells were significantly increased ($P < 0.05$) in the control compared with the mutant (Fig. 6G–I). To determine whether this effect was a result of increased radial glial progenitors, we counted pax6-labeled radial glia and found no significant difference between the control and the mutant (Fig. 6J–L).

Loss of *Tsc2* in radial glia caused causes myelin formation defects and increases oligodendrocytes

Advances in MRI imaging techniques have identified a variety of white matter defects in the brains of TSC patients (58,59). Diffusion tension MRI, which detects the direction and magnitude of water diffusion in tissues, has even identified microstructrural defects in normal-appearing white matter from TSC patients (59). Some of the most common white matter lesions identified in the brains of TSC patients were gliosis and hypomyelination. The neuron-specific *Tsc1* mouse

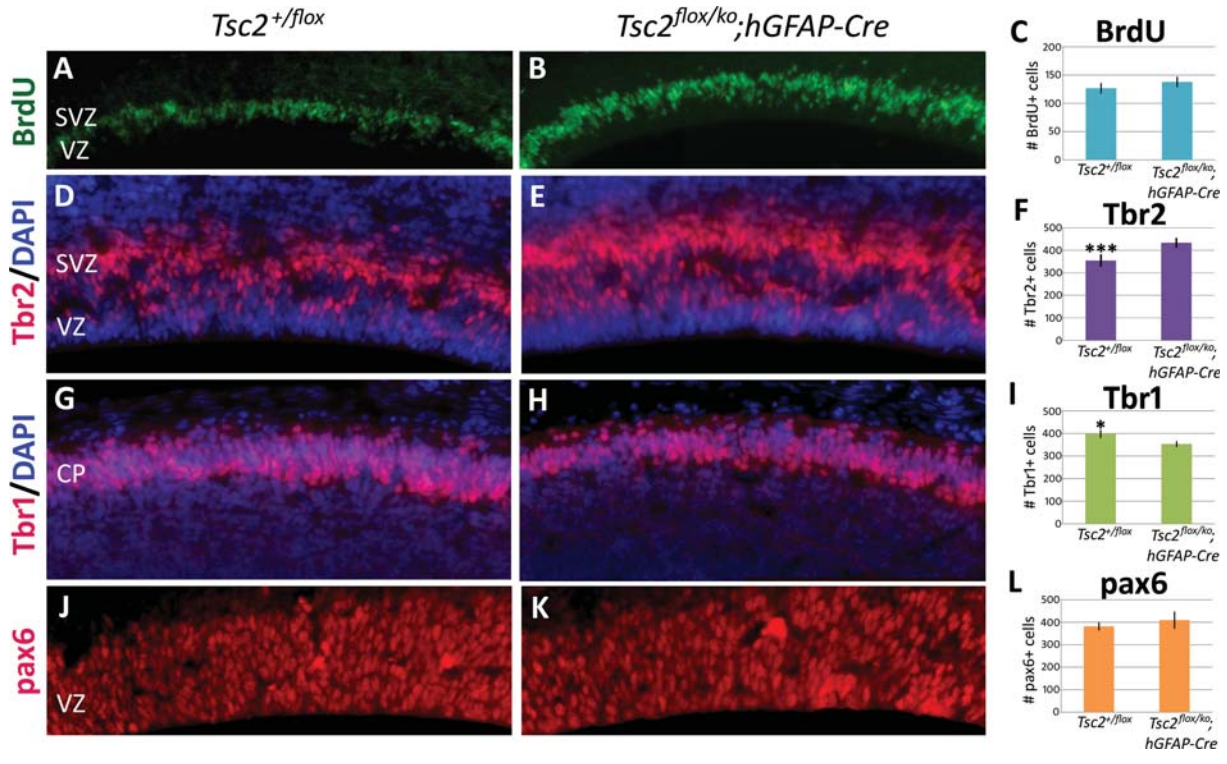

Figure 6. Cortical neural progenitor pool analysis at embryonic day E14.5. **(A–C)** BrdU pulse-labeling failed to detect any significant proliferative differences along the ventricles of the control and mutant embryos at E14.5 ($n = 6$). **(D–F)** Significantly more (F, $^{***}P < 0.0005$) Tbr2-labeled basal progenitor cells were found in the subventricular zone of the mutant (E) compared with the control (D) ($n = 6$). **(G–I)** The number of post-mitotic Tbr1-labeled neurons was significantly decreased (I, $^{*}P < 0.05$) in the control (G) ($n = 6$). **(J–L)** Radial glia numbers (L), as labeled by pax6, were not found to be significantly different between the control and the mutant (J) ($n = 4$). CP, cortical plate, SVZ, subventricular zone, VZ, ventricular zone. A, B, G and H taken at 20× magnification, D, E, J and K taken at 40×.

model demonstrated significant hypomyelination (37). To investigate white matter defects in our mutant mice, we performed immunohistochemistry for myelin basic protein (MBP). Myelination is progressing in control and mutant animals in the corpus callosum at P10 (Fig. 7A). In the mutant, myelination appeared to be discontinuous at several places. By P15, myelination had progressed, though there was a paucity of myelinated fibers in the more superficial layers of the cortex, as well as in the hippocampus (Fig. 7B). There was no significant difference between myelin patterns between P15 and P21. To assess whether defects in myelin-producing oligodendrocytes might have contributed to this phenotype, we performed immunohistochemistry to CC1, an oligodendrocyte marker. Interestingly, mutant mice had more oligodendrocytes than control (665 cells/mm^2 $\pm$ 46 versus 532 cell/mm^2 $\pm$ 35, $P = 0.05$). Double labeling with CC1 and pS6 revealed that a larger number of oligodendrocytes in the mutant have up-regulated mTORC1 activity (Fig. 7C and D). In spite of an increased number of activated oligidendrocytes, myelination does not proceed normally in mutant animals.

DISCUSSION

We have created a novel *Tsc2*-based brain-specific model of TSC by Cre-mediated ablation in radial glial progenitor cells. Consequently, all neurons and glia derived from Tsc2-null radial glia were devoid of Tsc2 and demonstrated mTORC1 activation, similar to the cells of human TSC brain lesions (18). The brains of the *Tsc2$^{flox/ko}$;hGFAP-Cre* mice exhibited many neuropathologic features of human TSC, such as cortical thickening, enlarged cells, lamination defects, heterotopias and abnormal myelination. Although there were no focal tubers *per se*, there were focal lesions in the hippocampus and the entire cerebral cortex had many characteristics of tubers. Our results support the neuroprogenitor hypothesis of TSC brain lesions (18,31). TSC is also considered a tumor suppressor disorder; however, LOH has been difficult to demonstrate for some human brain lesions (51,52). Our data demonstrate that LOH of *Tsc2* in radial glia model TSC neuropathology and support the two-hit hypothesis for the formation of human TSC brain lesions.

The *Tsc2$^{flox/ko}$;hGFAP-Cre* model differs significantly from the neuronal-specific *Tsc1$^{flox/ko}$;SynICre* mouse and the glial-specific *Tsc1$^{flox/flox}$;GFAP-Cre* mouse models of TSC in two important ways (36,37). First, the mouse homolog of the *TSC2* gene, associated with more severe human neurologic defects, was conditionally inactivated in this model. Secondly, since the *Tsc2* gene was deleted in radial glial progenitor cells, all their resulting neuronal and glial progeny were also lacking in Tsc2 activity as demonstrated by mTORC1 activation. The survival of these mice was more severely compromised than

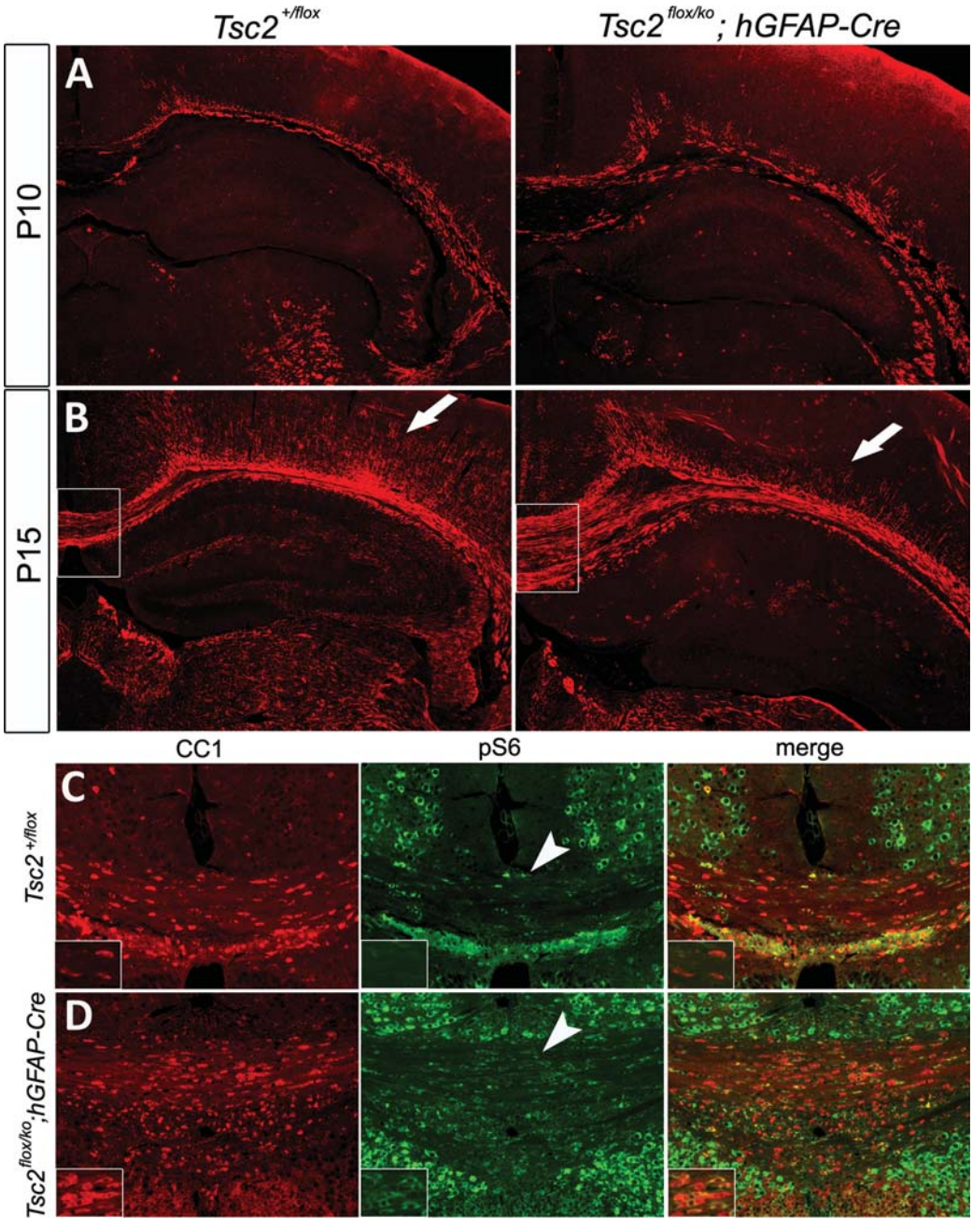

Figure 7. Post-natal developmental analysis of hypomyelination and oligodendrocytes in the mutant. **(A** and **B)** Immunostaining of MBP at P10 (A) and P15 (B) demonstrated a defect in myelin formation in the mutant cortex (arrows). **(C** and **D)** Oligodendrocyte analysis using CC1 revealed a 1.25-fold increase in CC1-labeled cells in the mutant ($n = 4$, data not shown) compared with the control. Colocalization of pS6 and CC1 (arrowheads) showed that most oligodendrocytes in the mutant had up-regulated mTORC1 activity.

the other neuronal and astrocyte-specific *Tsc1* brain-specific knockouts, dying between 3 and 4 weeks rather than 2–3 months of age (36,37). Although we have not performed EEG recordings of epileptiform activity, we have observed generalized seizures in several animals. When animals were found dead, they typically were in extensor posturing suggesting that they died from a tonic seizure. Future electrophysiologic studies will be required to understand the epilepsy that these animals have.

TSC has been considered a disorder of neuronal migration (6). The defects observed in the cerebral cortex and hippocampus provide evidence to support a neuronal migration defect. The lamination defects of the hippocampal pyramidal layer were similar to defects seen in mice with targeted disruptions of neuronal migration genes such as *Reelin*, *Lis1* and *Doublecortin* (60–62). The ring heterotopias also appeared to represent abnormal migration of neurons, glia and other unidentified cells. The presence of more Cux-1-expressing cells

in the deep layers of the mutant cortex, and the thickened ventricular zone of P0 mutant mice also suggested a neuronal migration defect. Further investigation into the role of the TSC complex in neuronal migration will be required, but this model should make *in vivo* developmental studies feasible.

The initial, striking feature of the brains of the TSC mice was the megalencephaly. The enlarged brains of these animals are reminiscent of the enlarged eye phenotype seen in the seminal studies in *Drosophila* that established the roles of the *Tsc1* and *Tsc2* genes in controlling cell and organ size (63,64). Hemimegalencephaly has also been reported as a rare manifestation of TSC (65,66). Cortical size is controlled by a delicate balance of proliferation, differentiation and apoptosis (67–69). The TSC complex has been demonstrated to regulate all these processes in different model systems. The developmental analysis indicated that the enlarged brain phenotype was predominantly a post-natal event. Minimal proliferation abnormalities were found in the cortex, whereas significantly increased PCNA-positive cells were found in the hippocampus. It appears that increased cell size and matrix are the principle determinants for the cortical enlargement, whereas hippocampal enlargement was dependent on both increased proliferation and increased cell size and matrix.

The differences in neuronal composition of the adult *Tsc2$^{flox/ko}$;hGFAP-Cre* cortex suggested that loss of Tsc2 might alter cell fate. Embryonic studies indicated that although total proliferation and radial glial cell numbers were unaffected at E14.5, there were notably more basal progenitor cells and fewer post-mitotic neurons in the mutant embryos. These findings indicate that loss of Tsc2 perturbs progenitor differentiation. Given the fewer early born post-mitotic neurons in the mutant embryo, it follows that there were fewer Layer VI FoxP2-positive neurons in the adult mutant cortex. However, although the large increase in basal progenitor cells in the mutant indicated that a similarly large increase in superficial-layer neurons should be present in the adult cortex, we were unable to find a significant increase in Cux-1-positive cells in Layers II–IV in the mice we have analyzed in the P21 cortex ($n = 6$). Recent studies have demonstrated that Tbr2-positive basal progenitor cells not only contribute to superficial cortical layers, but also deeper layers (70). Consequently, we hypothesize that loss of Tsc2 may increase pools of basal progenitor progeny in regions we have not studied, such as Layer V. Though we have not been able to detect apoptosis at E16.5, P5 or P10, we cannot completely exclude cell death of basal progenitors or their progeny as factors that contribute to the final P21 mutant brain.

Astrocytes can become reactive in response to a variety of CNS pathologies such as infection, ischemia or neurodegenerative disease (71,72). This reactive gliosis is accompanied by morphologic and cell physiologic changes, most notably, the up-regulation of intermediate filament proteins such as vimentin and GFAP. Cortical tubers contain characteristic giant cells surrounded by a severe astrogliosis. The cause of this TSC-associated astrogliosis is unknown, but suggests that dysfunctional, reactive astrocytes may be important in TSC neuropathology (55). The *Tsc2$^{flox/ko}$;hGFAP-Cre* mice displayed an extensive astrogliosis throughout the cortex and hippocampus, similar to the human disease. Though the giant cell is a hallmark feature of tubers, human and animal studies suggest that dysfunctional astrocytes may be a major site of neuropathology of TSC (36,55). This new mouse model will allow further assessment of the role of activated astrocytes in TSC pathology.

Brain myelination is a process whereby the membranes of oligodendrocytes wrap around and extend along neuronal axons (73). Normal myelination appears to rely not solely on oligodendrocytes, but also upon the correct signals from target axons (74). Abnormal myelination has recently been found to be another pathologic feature in the brains of TSC patients (58,59). The *Tsc2$^{flox/ko}$;hGFAP-Cre* mice also showed abnormalities in the progression of myelination that resulted in an undermyelinated cerebral cortex and hippocampus. Abnormalities in neurons and/or oligodendrocytes may have caused these defects as both cell populations demonstrated mTORC1 activation. Interestingly, the neuronal Tsc1 model mouse, in which post-mitotic neurons are deleted for Tsc1, also demonstrated very similar defects in myelination (37). Those data suggested that loss of Tsc1 disrupted neuronal signals that are crucial for the correct progression of myelination. Since both models demonstrate similar myelination defects, it is likely that the neuronal absence of Tsc2 is a major cause for the aberrant myelination. Future co-culture studies will be required to assess the effects of the TSC complex on the interplay between oligodendrocytes and neurons and the regulation of myelination.

The *Tsc2$^{flox/ko}$;hGFAP-Cre* model of TSC suggests that the radial glial cell might be a cellular site for LOH in human TSC brain lesions. Although our results do not preclude LOH in other progenitor cells such as neuroepithelial or basal progenitor cells, the resultant phenotype suggests a crucial role for tight regulation of the mTORC1 pathway in radial glial progenitor differentiation and neuronal migration. Loss of mTORC1 regulation plays a role in other developmental brain disorders such as neurofibromatosis type 1 and PTEN-associated macrocephaly (75,76). Further study of the developmental defects in radial glia caused by loss of TSC-regulated mTORC1 should provide insight not only into TSC, but also many other neurodevelopmental defects. The *Tsc2$^{flox/ko}$;hGFAP-Cre* mouse demonstrated activation of mTORC1, so rapamycin treatment should rescue some of the neuropathology. Since neurons and glia are affected in this model, it will be interesting to assess whether there is a differential cellular response to rapamycin treatment. The creation of a *Tsc1$^{flox/ko}$;hGFAP-Cre* is in progress and will allow a comparison with the present model to provide a possible biologic basis for the differences in severity between patients with *TSC1* versus *TSC2* mutations. This *Tsc2*-based model also broadens the availability of models for the preclinical testing of established and novel drugs for the treatment of TSC and related disorders.

MATERIALS AND METHODS

Mice and genotyping

All animal experimentation was approved by the UTHSC Animal Welfare Committee. Mice were in a mixed 129 and

C57/Bl6 background. *Tsc2*$^{+/flox}$, *Tsc2*$^{+/ko}$ and *hGFAP-Cre* mice have been previously described (41,48,49). Mice were genotyped for *Tsc2* alleles using three primers in one PCR reaction: KO1: 5′-GCAGCAGGTCTGCAGTGAAT-3′, KO2: 5′-CCTCCTGCATGGAGTTGAGT-3′; WT2: 5′-CAGGCAT GTCTGGAGTCTTG -3′.

Band sizes were wild-type (390 bp), *Tsc2*^{flox} (434 bp) and *Tsc2*^{ko} (547 bp). Cre primers: CreF: 5′-GGACATGTTCA GGGATCTCCAGGC-3′, CreR: 5′-CGACGATGAAGCA TGTTTAGCTG-3′, RapA: 5′-AGGACTGGGTGGCTTCC AACTCCCAGACAC-3′, RapB: 5′-AGCTTCTCATTGCTGC GCGCCAGGTTCAGG-3′. Band sizes were Cre (219 bp) and Rap (590 bp) as a positive control band. Cre and Rap primers were generously provided by the laboratory of Richard Behringer.

Histological studies

Adult mice were deeply anesthetized before undergoing transcardiac perfusion with PBS and then with 4% paraformaldehyde (PFA). Mouse brains were post-fixed in PFA overnight and stored in 70% ethanol prior to embedding in paraffin. Paraffin blocks were sectioned at 5 μm. For embryo analysis, the day of the vaginal plug was 0.5. Dams were anesthetized with 2.5% avertin and killed by cervical dislocation before embryos were dissected into cold PBS and staged. A small piece of the embryo was used for genotyping. Embryos were fixed in PFA 4–6 h and washed in 1× PBS before being stored in 70% ethanol and embedded in paraffin. Slides were rehydrated, stained with routine H&E, and coverslipped.

Immunofluorescence was performed by blocking in 10% serum from animal in which secondary antibody was raised and 0.05% Triton X-100 in 1× PBS for 1 h. Primary antibody was allowed to incubate overnight at 4°C. Sections were washed in 1× PBS followed by secondary antibody incubation for 1 h. Tissue was directly visualized for fluorescence-conjugated secondary antibodies. Tissue images were examined using an Olympus BX51 or IX81 microscope and captured with a Qimaging RETIGA-2000RV digital camera or a Bio-Rad 1024 MP confocal microscope. Digital images were then processed using Adobe Photoshop (San Jose, CA, USA).

Antibodies

The antibodies used for immunohistochemistry were as follows: Pax6 (1:2000, Developmental Studies Hybridoma Bank, Iowa City, IA, USA), phosphorylated (Ser 240/244) S6 (1:100, Cell Signaling Technology, Bedford, MA, USA), Cux-1 (1:50, Santa Cruz Biotechnology, Santa Cruz, CA, USA), FoxP2 (1:4000, Abcam, Cambridge, MA, USA), BrdU (1:50, Becton Dickinson, San Jose, CA, USA), GFAP (1:400, Sigma), CC1 (1:5, Calbiochem, Gibbstown, NJ, USA), S100 (1:100, DakoCytomation, Denmark and 1:500, Abcam), PCNA (1:50, Santa Cruz) and NeuN (1:100), Tbr2 (1:2000), Tbr1 (1:500) and MBP (1:200) from Millipore, Billerica, MA, USA. Prolong Gold antifade reagent with DAPI (Invitrogen, Eugene, OR, USA) was used for DAPI staining and coverslipping of post-natal tissue. Embryonic tissue was stained with Hoechst 33258 (Invitrogen) after removal of the secondary antibody and coverslipped using Fluoromount-G (SouthernBiotech, Birmingha, AL, USA). The antibodies used for immunoblotting were: tuberin (1:1000), hamartin (1:1000), pS6 (1:2000) and α-tubulin (1:1000), from Cell Signaling.

Quantitative analysis

Two or three serial sections from each mouse were used for analysis unless otherwise noted. For post-natal cell counts, equal-sized images spanning the thickness of the somatosensory cortex were taken at the same lateral distance from the midline. Count results were corrected to represent a percentage of cells in the cortex in order to account for differences in total cortex size. For embryo counts, equal-sized images spanning most of the length of the lateral ventricles were used. Marker-labeled cells with visible nuclei were manually counted using Photoshop and ImageJ v1.38x (W. Rasband, National Institutes of Health, Bethesda, MD, USA). For neuron cell size determination, the cortex was divided into five equal bins from the bottom of Layer I to the bottom of Layer VI. In one section each from three pairs of control and mutant mice, 50 NeuN-labeled neurons from Bin 3 were outlined and filled using Photoshop and area was analyzed in micrometers using ImageJ. For DG area calculation, one section each from three pairs of mice were stained with H&E. DG cell images were captured using a 60× objective and cells near the midline of the DG were outlined for area calculation in the same manner. Data were analyzed using repeated-measures ANOVA in SPSS (Chicago, IL, USA) and Microsoft Excel (Seattle, WA, USA).

Protein analysis

Whole cell lysates were made from P21 cerebral cortex and hippocampus that were quick-frozen in liquid nitrogen. Samples were homogenized in a dounce homogenizer with 10 volumes of Ripa buffer with protease inhibitor cocktail and phosphatase inhibitor cocktail (Sigma). Lysates were centrifuged at 4°C, sonicated and frozen until use. Protein concentrations were determined with a BCA reagent kit (Pierce, ThermoFisher Scientific, Rockford, IL, USA). Equal amounts of protein were separated on a denaturing 4–12% gradient gel (Invitrogen) and transferred to nitrocellulose. The membrane was cut into sections and each section probed with different antibodies using a stripping procedure after each experiment if necessary. Secondary antibodies were horseradish peroxidase conjugated. Visualization was conducted with an ECL kit (Amersham, Piscataway, NJ, USA).

ACKNOWLEDGEMENTS

We would like to thank Drs. Seonhee Kim, Seo-Hee Cho and S. Shahrukh Hashmi for their helpful suggestions on this manuscript.

Conflict of Interest statement. None declared.

FUNDING

This work is supported by NIH grant to M.J.G. (RO1NS060804) and the Tuberous Sclerosis Alliance. Funding to Pay the Open Access Charge was provided by the National Institutes of Health.

REFERENCES

1. Crino, P.B., Nathanson, K.L. and Henske, E.P. (2006) The tuberous sclerosis complex. *N. Engl. J. Med.*, **355**, 1345–1356.
2. Consortium. (1993) Identification and characterization of the tuberous sclerosis gene on chromosome 16. *Cell*, **75**, 1305–1315.
3. van Slegtenhorst, M., de Hoogt, R., Hermans, C., Nellist, M., Janssen, B., Verhoef, S., Lindhout, D., van den Ouweland, A., Halley, D., Young, J. *et al.* (1997) Identification of the tuberous sclerosis gene TSC1 on chromosome 9q34. *Science*, **277**, 805–808.
4. Cheadle, J.P., Reeve, M.P., Sampson, J.R. and Kwiatkowski, D.J. (2000) Molecular genetic advances in tuberous sclerosis. *Hum. Genet.*, **107**, 97–114.
5. Chan, J.A., Zhang, H., Roberts, P.S., Jozwiak, S., Wieslawa, G., Lewin-Kowalik, J., Kotulska, K. and Kwiatkowski, D.J. (2004) Pathogenesis of tuberous sclerosis subependymal giant cell astrocytomas: biallelic inactivation of TSC1 or TSC2 leads to mTOR activation. *J. Neuropathol. Exp. Neurol*, **63**, 1236–1242.
6. Gomez, M.R. (1999) *Tuberous Sclerosis Complex*, 3rd edn. Oxford University Press, New York.
7. DiMario, F.J. Jr. (2004) Brain abnormalities in tuberous sclerosis complex. *J. Child Neurol.*, **19**, 650–657.
8. Thiele, E.A. (2004) Managing epilepsy in tuberous sclerosis complex. *J. Child Neurol.*, **19**, 680–686.
9. Prather, P. and de Vries, P.J. (2004) Behavioral and cognitive aspects of tuberous sclerosis complex. *J. Child Neurol.*, **19**, 666–674.
10. Smalley, S.L. (1998) Autism and tuberous sclerosis. *J. Autism Dev. Disord.*, **28**, 407–414.
11. Tapon, N., Ito, N., Dickson, B.J., Treisman, J.E. and Hariharan, I.K. (2001) The *Drosophila* tuberous sclerosis complex gene homologs restrict cell growth and cell proliferation. *Cell*, **105**, 345–355.
12. Sarbassov, D.D., Ali, S.M. and Sabatini, D.M. (2005) Growing roles for the mTOR pathway. *Curr. Opin. Cell Biol.*, **17**, 596–603.
13. Gao, X., Zhang, Y., Arrazola, P., Hino, O., Kobayashi, T., Yeung, R.S., Ru, B. and Pan, D. (2002) Tsc tumour suppressor proteins antagonize amino-acid-TOR signalling. *Nat. Cell Biol.*, **4**, 699–704.
14. Garami, A., Zwartkruis, F.J., Nobukuni, T., Joaquin, M., Roccio, M., Stocker, H., Kozma, S.C., Hafen, E., Bos, J.L. and Thomas, G. (2003) Insulin activation of Rheb, a mediator of mTOR/S6K/4E-BP signaling, is inhibited by TSC1 and 2. *Mol. Cell*, **11**, 1457–1466.
15. Zhang, Y., Gao, X., Saucedo, L.J., Ru, B., Edgar, B.A. and Pan, D. (2003) Rheb is a direct target of the tuberous sclerosis tumour suppressor proteins. *Nat. Cell Biol.*, **5**, 578–581.
16. Kim, D.H., Sarbassov, D.D., Ali, S.M., Latek, R.R., Guntur, K.V., Erdjument-Bromage, H., Tempst, P. and Sabatini, D.M. (2003) GbetaL, a positive regulator of the rapamycin-sensitive pathway required for the nutrient-sensitive interaction between raptor and mTOR. *Mol. Cell*, **11**, 895–904.
17. Kim, D.H., Sarbassov, D.D., Ali, S.M., King, J.E., Latek, R.R., Erdjument-Bromage, H., Tempst, P. and Sabatini, D.M. (2002) mTOR interacts with raptor to form a nutrient-sensitive complex that signals to the cell growth machinery. *Cell*, **110**, 163–175.
18. Crino, P.B. (2004) Molecular pathogenesis of tuber formation in tuberous sclerosis complex. *J. Child Neurol.*, **19**, 716–725.
19. Paghdal, K.V. and Schwartz, R.A. (2007) Sirolimus (rapamycin): from the soil of Easter Island to a bright future. *J. Am. Acad. Dermatol.*, **57**, 1046–1050.
20. Kenerson, H., Dundon, T.A. and Yeung, R.S. (2005) Effects of rapamycin in the Eker rat model of tuberous sclerosis complex. *Pediatr. Res.*, **57**, 67–75.
21. Lee, L., Sudentas, P., Donohue, B., Asrican, K., Worku, A., Walker, V., Sun, Y., Schmidt, K., Albert, M.S., El-Hashemite, N. *et al.* (2005) Efficacy of a rapamycin analog (CCI-779) and IFN-gamma in tuberous sclerosis mouse models. *Genes Chromosomes Cancer*, **42**, 213–227.
22. Kwiatkowski, D.J., Zhang, H., Bandura, J.L., Heiberger, K.M., Glogauer, M., el-Hashemite, N. and Onda, H. (2002) A mouse model of TSC1 reveals sex-dependent lethality from liver hemangiomas, and up-regulation of p70S6 kinase activity in Tsc1 null cells. *Hum. Mol. Genet.*, **11**, 525–534.
23. Manning, B.D., Tee, A.R., Logsdon, M.N., Blenis, J. and Cantley, L.C. (2002) Identification of the tuberous sclerosis complex-2 tumor suppressor gene product tuberin as a target of the phosphoinositide 3-kinase/akt pathway. *Mol. Cell*, **10**, 151–162.
24. Zeng, L.H., Xu, L., Gutmann, D.H. and Wong, M. (2008) Rapamycin prevents epilepsy in a mouse model of tuberous sclerosis complex. *Ann. Neurol.*, **63**, 444–453.
25. Meikle, L., Pollizzi, K., Egnor, A., Kramvis, I., Lane, H., Sahin, M. and Kwiatkowski, D.J. (2008) Response of a neuronal model of tuberous sclerosis to mammalian target of rapamycin (mTOR) inhibitors: effects on mTORC1 and Akt signaling lead to improved survival and function. *J. Neurosci.*, **28**, 5422–5432.
26. Bissler, J.J., McCormack, F.X., Young, L.R., Elwing, J.M., Chuck, G., Leonard, J.M., Schmithorst, V.J., Laor, T., Brody, A.S., Bean, J. *et al.* (2008) Sirolimus for angiomyolipoma in tuberous sclerosis complex or lymphangioleiomyomatosis. *N. Engl. J. Med.*, **358**, 140–151.
27. Franz, D.N., Leonard, J., Tudor, C., Chuck, G., Care, M., Sethuraman, G., Dinopoulos, A., Thomas, G. and Crone, K.R. (2006) Rapamycin causes regression of astrocytomas in tuberous sclerosis complex. *Ann. Neurol.*, **59**, 490–498.
28. Park, S.H., Pepkowitz, S.H., Kerfoot, C., De Rosa, M.J., Poukens, V., Wienecke, R., DeClue, J.E. and Vinters, H.V. (1997) Tuberous sclerosis in a 20-week gestation fetus: immunohistochemical study. *Acta Neuropathol.*, **94**, 180–186.
29. Crino, P.B., Trojanowski, J.Q., Dichter, M.A. and Eberwine, J. (1996) Embryonic neuronal markers in tuberous sclerosis: single-cell molecular pathology. *Proc. Natl Acad. Sci. USA*, **93**, 14152–14157.
30. Hirose, T., Scheithauer, B.W., Lopes, M.B., Gerber, H.A., Altermatt, H.J., Hukee, M.J., VandenBerg, S.R. and Charlesworth, J.C. (1995) Tuber and subependymal giant cell astrocytoma associated with tuberous sclerosis: an immunohistochemical, ultrastructural, and immunoelectron and microscopic study. *Acta Neuropathol.*, **90**, 387–399.
31. Scheidenhelm, D.K. and Gutmann, D.H. (2004) Mouse models of tuberous sclerosis complex. *J. Child Neurol.*, **19**, 726–733.
32. Kobayashi, T., Minowa, O., Kuno, J., Mitani, H., Hino, O. and Noda, T. (1999) Renal carcinogenesis, hepatic hemangiomatosis, and embryonic lethality caused by a germ-line Tsc2 mutation in mice. *Cancer Res.*, **59**, 1206–1211.
33. Kobayashi, T., Minowa, O., Sugitani, Y., Takai, S., Mitani, H., Kobayashi, E., Noda, T. and Hino, O. (2001) A germ-line Tsc1 mutation causes tumor development and embryonic lethality that are similar, but not identical to, those caused by Tsc2 mutation in mice. *Proc. Natl Acad. Sci. USA*, **98**, 8762–8767.
34. Onda, H., Lueck, A., Marks, P.W., Warren, H.B. and Kwiatkowski, D.J. (1999) Tsc2(+/−) mice develop tumors in multiple sites that express gelsolin and are influenced by genetic background. *J. Clin. Invest.*, **104**, 687–695.
35. Wilson, C., Idziaszczyk, S., Parry, L., Guy, C., Griffiths, D.F., Lazda, E., Bayne, R.A., Smith, A.J., Sampson, J.R. and Cheadle, J.P. (2005) A mouse model of tuberous sclerosis 1 showing background specific early post-natal mortality and metastatic renal cell carcinoma. *Hum. Mol. Genet.*, **14**, 1839–1850.
36. Uhlmann, E.J., Wong, M., Baldwin, R.L., Bajenaru, M.L., Onda, H., Kwiatkowski, D.J., Yamada, K. and Gutmann, D.H. (2002) Astrocyte-specific TSC1 conditional knockout mice exhibit abnormal neuronal organization and seizures. *Ann. Neurol.*, **52**, 285–296.
37. Meikle, L., Talos, D.M., Onda, H., Pollizzi, K., Rotenberg, A., Sahin, M., Jensen, F.E. and Kwiatkowski, D.J. (2007) A mouse model of tuberous sclerosis: neuronal loss of Tsc1 causes dysplastic and ectopic neurons, reduced myelination, seizure activity, and limited survival. *J. Neurosci.*, **27**, 5546–5558.
38. Wang, Y., Greenwood, J.S., Calcagnotto, M.E., Kirsch, H.E., Barbaro, N.M. and Baraban, S.C. (2007) Neocortical hyperexcitability in a human case of tuberous sclerosis complex and mice lacking neuronal expression of TSC1. *Ann. Neurol.*, **61**, 139–152.
39. Dabora, S.L., Jozwiak, S., Franz, D.N., Roberts, P.S., Nieto, A., Chung, J., Choy, Y.S., Reeve, M.P., Thiele, E., Egelhoff, J.C. *et al.* (2001) Mutational analysis in a cohort of 224 tuberous sclerosis patients indicates

increased severity of TSC2, compared with TSC1, disease in multiple organs. *Am. J. Hum. Genet.*, **68**, 64–80.
40. Au, K.S., Williams, A.T., Roach, E.S., Batchelor, L., Sparagana, S.P., Delgado, M.R., Wheless, J.W., Baumgartner, J.E., Roa, B.B., Wilson, C.M. *et al.* (2007) Genotype/phenotype correlation in 325 individuals referred for a diagnosis of tuberous sclerosis complex in the United States. *Genet. Med.*, **9**, 88–100.
41. Hernandez, O., Way, S., McKenna, J. III and Gambello, M.J. (2007) Generation of a conditional disruption of the Tsc2 gene. *Genesis*, **45**, 101–106.
42. Campbell, K. and Gotz, M. (2002) Radial glia: multi-purpose cells for vertebrate brain development. *Trends Neurosci.*, **25**, 235–238.
43. Noctor, S.C., Flint, A.C., Weissman, T.A., Dammerman, R.S. and Kriegstein, A.R. (2001) Neurons derived from radial glial cells establish radial units in neocortex. *Nature*, **409**, 714–720.
44. Noctor, S.C., Flint, A.C., Weissman, T.A., Wong, W.S., Clinton, B.K. and Kriegstein, A.R. (2002) Dividing precursor cells of the embryonic cortical ventricular zone have morphological and molecular characteristics of radial glia. *J. Neurosci.*, **22**, 3161–3173.
45. Gotz, M. and Pinto, L. (2007) Radial glial cell heterogeneity—the source of diverse progeny in the CNS. *Prog. Neurobiol.*, **83**, 2–23.
46. Noctor, S., Martinez-Cerdeno, V., Ivic, L. and Kriegstein, A. (2004) Cortical neurons arise in symmetric and asymmetric division zones and migrate through specific phases. *Nat. Neurosci.*, **7**, 136–144.
47. Haubensak, W., Attardo, A., Denk, W. and Huttner, W. (2004) Neurons arise in the basal neuroepithelium of the early mammalian telencephalon: a major site of neurogenesis. *Proc. Natl Acad. Sci. USA*, **101**, 3196–3201.
48. Zhuo, L., Theis, M., Alvarez-Maya, I., Brenner, M., Willecke, K. and Messing, A. (2001) hGFAP-cre transgenic mice for manipulation of glial and neuronal function in vivo. *Genesis*, **31**, 85–94.
49. Malatesta, P., Hack, M.A., Hartfuss, E., Kettenmann, H., Klinkert, W., Kirchhoff, F. and Gotz, M. (2003) Neuronal or glial progeny: regional differences in radial glia fate. *Neuron*, **37**, 751–764.
50. Ohkubo, Y., Uchida, A.O., Shin, D., Partanen, J. and Vaccarino, F.M. (2004) Fibroblast growth factor receptor 1 is required for the proliferation of hippocampal progenitor cells and for hippocampal growth in mouse. *J. Neurosci.*, **24**, 6057–6069.
51. Jozwiak, J. and Jozwiak, S. (2007) Giant cells: contradiction to two-hit model of tuber formation? *Cell Mol. Neurobiol.*, **27**, 251–261.
52. Mizuguchi, M., Mori, M., Nozaki, Y., Momoi, M.Y., Itoh, M., Takashima, S. and Hino, O. (2004) Absence of allelic loss in cytomegalic neurons of cortical tuber in the Eker rat model of tuberous sclerosis. *Acta Neuropathol.*, **107**, 47–52.
53. Benvenuto, G., Li, S., Brown, S.J., Braverman, R., Vass, W.C., Cheadle, J.P., Halley, D.J., Sampson, J.R., Wienecke, R. and DeClue, J.E. (2000) The tuberous sclerosis-1 (TSC1) gene product hamartin suppresses cell growth and augments the expression of the TSC2 product tuberin by inhibiting its ubiquitination. *Oncogene*, **19**, 6306–6316.
54. Englund, C., Fink, A., Lau, C., Pham, D., Daza, R.A., Bulfone, A., Kowalczyk, T. and Hevner, R.F. (2005) Pax6, Tbr2 and Tbr1 are expressed sequentially by radial glia, intermediate progenitor cells, and postmitotic neurons in developing neocortex. *J. Neurosci.*, **25**, 247–251.
55. Sosunov, A.A., Wu, X., Weiner, H.L., Mikell, C.B., Goodman, R.R., Crino, P.D. and McKhann, G.M. II (2008). Tuberous sclerosis: a primary pathology of astrocytes? *Epilepsia*, **49** (Suppl. 2), 53–62.
56. Nieto, M., Monuki, E.S., Tang, H., Imitola, J., Haubst, N., Khoury, S.J., Cunningham, J., Gotz, M. and Walsh, C.A. (2004) Expression of Cux-1 and Cux-2 in the subventricular zone and upper layers II–IV of the cerebral cortex. *J. Comp. Neurol.*, **479**, 168–180.
57. Ferland, R.J., Cherry, T.J., Preware, P.O., Morrisey, E.E. and Walsh, C.A. (2003) Characterization of Foxp2 and Foxp1 mRNA and protein in the developing and mature brain. *J. Comp. Neurol.*, **460**, 266–279.
58. Griffiths, P.D., Bolton, P. and Verity, C. (1998) White matter abnormalities in tuberous sclerosis complex. *Acta Radiol.*, **39**, 482–486.
59. Makki, M.I., Chugani, D.C., Janisse, J. and Chugani, H.T. (2007) Characteristics of abnormal diffusivity in normal-appearing white matter investigated with diffusion tensor MR imaging in tuberous sclerosis complex. *Am. J. Neuroradiol.*, **28**, 1662–1667.
60. Del Rio, J.A., Heimrich, B., Borrell, V., Forster, E., Drakew, A., Alcantara, S., Nakajima, K., Miyata, T., Ogawa, M., Mikoshiba, K. *et al.* (1997) A role for Cajal–Retzius cells and reelin in the development of hippocampal connections. *Nature*, **385**, 70–74.
61. Hirotsune, S., Fleck, M.W., Gambello, M.J., Bix, G.J., Chen, A., Clark, G.D., Ledbetter, D.H., McBain, C.J. and Wynshaw-Boris, A. (1998) Graded reduction of Pafah1b1 (Lis1) activity results in neuronal migration defects and early embryonic lethality. *Nat. Genet.*, **19**, 333–339.
62. Corbo, J.C., Deuel, T.A., Long, J.M., LaPorte, P., Tsai, E., Wynshaw-Boris, A. and Walsh, C.A. (2002) Doublecortin is required in mice for lamination of the hippocampus but not the neocortex. *J. Neurosci.*, **22**, 7548–7557.
63. Gao, X. and Pan, D. (2001) TSC1 and TSC2 tumor suppressors antagonize insulin signaling in cell growth. *Genes Dev.*, **15**, 1383–1392.
64. Potter, C.J., Huang, H. and Xu, T. (2001) *Drosophila* Tsc1 functions with Tsc2 to antagonize insulin signaling in regulating cell growth, cell proliferation, and organ size. *Cell*, **105**, 357–368.
65. Galluzzi, P., Cerase, A., Strambi, M., Buoni, S., Fois, A. and Venturi, C. (2002) Hemimegalencephaly in tuberous sclerosis complex. *J. Child Neurol.*, **17**, 677–680.
66. Cartwright, M.S., McCarthy, S.C. and Roach, E.S. (2005) Hemimegalencephaly and tuberous sclerosis complex. *Neurology*, **64**, 1634.
67. Chenn, A. and Walsh, C.A. (2002) Regulation of cerebral cortical size by control of cell cycle exit in neural precursors. *Science*, **297**, 365–369.
68. Tang, B.L. (2006) Molecular genetic determinants of human brain size. *Biochem. Biophys. Res. Commun.*, **345**, 911–916.
69. Kuida, K., Haydar, T.F., Kuan, C.Y., Gu, Y., Taya, C., Karasuyama, H., Su, M.S., Rakic, P. and Flavell, R.A. (1998) Reduced apoptosis and cytochrome c-mediated caspase activation in mice lacking caspase 9. *Cell*, **94**, 325–337.
70. Sessa, A., Mao, C., Hadjantonakis, A., Klein, W. and Broccoli, V. (2008) Tbr2 directs conversion of radial glia into basal precursors and guides neuronal amplification by indirect neurogenesis in the developing cortex. *Neuron*, **60**, 56–69.
71. Correa-Cerro, L.S. and Mandell, J.W. (2007) Molecular mechanisms of astrogliosis: new approaches with mouse genetics. *J. Neuropathol. Exp. Neurol.*, **66**, 169–176.
72. Pekny, M. and Nilsson, M. (2005) Astrocyte activation and reactive gliosis. *Glia*, **50**, 427–434.
73. Simons, M. and Trotter, J. (2007) Wrapping it up: the cell biology of myelination. *Curr. Opin. Neurobiol.*, **17**, 533–540.
74. Sher, F., Balasubramanian, V., Boddeke, E. and Copray, S. (2008) Oligodendrocyte differentiation and implantation: new insights for remyelinating cell therapy. *Curr. Opin. Neurol.*, **21**, 607–614.
75. Lee, M.J. and Stephenson, D.A. (2007) Recent developments in neurofibromatosis type 1. *Curr. Opin. Neurol.*, **20**, 135–141.
76. Butler, M.G., Dasouki, M.J., Zhou, X.P., Talebizadeh, Z., Brown, M., Takahashi, T.N., Miles, J.H., Wang, C.H., Stratton, R., Pilarski, R. *et al.* (2005) Subset of individuals with autism spectrum disorders and extreme macrocephaly associated with germline PTEN tumour suppressor gene mutations. *J. Med. Genet.*, **42**, 318–321.